"Zincone" Zinc Oxide−Organic Hybrid Polymer Thin Films Formed by Molecular Layer Deposition

Qing Peng, Bo Gong, Ryan M. VanGundy, and Gregory N. Parsons*

Department of Chemical and Biomolecular Engineering, North Carolina State University, Raleigh, North Carolina 27695

Received July 27, 2008. Revised Manuscript Received December 8, 2008

Hybrid organic−inorganic polymer thin films of the form $(-O-Zn-O-C_2H_4-)_n$ have been deposited from diethyl zinc and ethylene glycol using molecular layer deposition (MLD) over a range of substrate temperatures between 100 and 170 °C. Infrared transmission confirms that the films consist of Zn−O and ethylene-oxide units. In analogy with known alucone polymers of the form $(-O-Al-O-R-)_n$, the zinc-based hybrid material is an example of a "zincone" polymer. In situ quartz crystal microbalance analysis indicated that the sequential surface reactions of diethyl zinc and ethylene glycol are sufficiently self-limiting and saturating to enable well-controlled MLD growth. Quantitative analysis of in situ quartz crystal microbalance and film thickness results indicate that ethylene glycol molecules can undergo a "double reaction" where the OH groups on both ends of the diol react with available $Zn-C_2H_5$ surface sites to produce a relatively inert bridging alkane. The mass uptake per MLD cycle during Zn−hybrid film deposition decreases with increasing reaction temperature. Infrared transmission spectroscopy also shows that Zn−organic hybrid films are stable in dry air. However, the as-deposited ZnO−hybrid material could be hydrolyzed by H_2O (for example, in ambient) resulting in films consisting of zinc oxide and zinc hydroxide with some carbon remnants. Spectroscopic ellipsometry indicates the thickness of hydrolyzed films increases linearly with reaction cycles, and scanning probe and transmission electron microscopy images show the hydrolyzed ZnO−hybrid film coating is uniform and conformal. The transmission electron micrographs also show the hydrolyzed Zn−hybrid films contain nanoscale porosity. These results suggest new pathways to fabricate organic−inorganic hybrid materials, including metal-organic framework structures.

1. Introduction

Advances in chemical synthesis and thin film processing techniques are opening new approaches to prepare functional materials with well-defined composition, uniformity, and conformality. Atomic layer deposition (ALD),[1−5] for example, employing a repeated binary sequence of self-limiting monolayer deposition reactions, has been applied to a variety of inorganic metals and metal compounds for advanced electronic and optical applications.[6−12] Molecular layer deposition (MLD) expands upon the chemical concepts of ALD to integrate organic monomer and molecular building blocks into oligomeric and polymeric thin film structures with precise control of film thickness.[13−18] Recently, a combination of ALD and MLD approaches has been used to deposit several examples of hybrid organic−inorganic thin films, including compounds of aluminum, silicon, titanium, and others.[19−22] Some organic−inorganic hybrid materials are referred to as coordination polymers, or metal-organic framework solids, built up of repeating metal−ligand−metal

* Corresponding author: parsons@ncsu.edu.

(1) Lujala, V.; Skarp, J.; Tammenmaa, M.; Suntola, T. In *Atomic Layer Epitaxy Growth of Doped Zinc-Oxide Thin-Films from Organometals*; proceedings of the 3rd International Symposium on Atomic Layer Epitaxy and Related Surface Processes (ALE-3), Sendai, Japan, May 25−27, 1994; Elsevier Science: Amsterdam, 1994; p 34.
(2) Tammenmaa, M.; Koskinen, T.; Hiltunen, L.; Niinisto, L.; Leskela, M. *Thin Solid Films* **1985**, *124*, 125.
(3) Ahonen, M.; Pessa, M.; Suntola, T. *Thin Solid Films* **1980**, *65*, 301.
(4) George, S. M.; Ott, A. W.; Klaus, J. W. *J. Phys. Chem.* **1996**, *100*, 13121.
(5) Ritala, M.; Leskela, M. Atomic Layer Deposition. In *Handbook of Thin Film Materials*; Nalwa, H. S. Ed.; Academic Press: San Diego:, 2001; Vol. 1, p 103.
(6) Elam, J. W.; George, S. M. *Chem. Mater.* **2003**, *15*, 1020.
(7) Leskela, M.; Ritala, M. *Angew. Chem., Int. Ed.* **2003**, *42*, 5548.
(8) Chen, P.; Mitsui, T.; Farmer, D. B.; Golovchenko, J.; Gordon, R. G.; Branton, D. *Nano Lett.* **2004**, *4*, 1333.
(9) Kim, H. *J. Vac. Sci. Technol., B* **2003**, *21*, 2231.
(10) Gordon, R. G.; Becker, J.; Hausmann, D.; Suh, S. *Chem. Mater.* **2001**, *13*, 2463.
(11) Peng, Q.; Sun, X. Y.; Spagnola, J. C.; Hyde, G. K.; Spontak, R. J.; Parsons, G. N. *Nano Lett.* **2007**, *7*, 719.
(12) Knez, M.; Knielsch, K.; Niinisto, L. *Adv. Mater.* **2007**, *19*, 3425.
(13) Yoshimura, T.; Tetsuura, S.; Sotoyama, W. *Appl. Phys. Lett.* **1991**, *59*, 482.
(14) Kubono, A.; Okui, N.; Tanaka, K.; Umemoto, S.; Sakai, T. *Thin Solid Films* **1991**, *199*, 385.
(15) Kim, A.; Filler, M. A.; Kim, S.; Bent, S. F. *J. Am. Chem. Soc.* **2005**, *127*, 6123.
(16) Putkonen, M.; Harjuoja, J.; Sajavaara, T.; Niinisto, L. *J. Mater. Chem.* **2007**, *17*, 664.
(17) Du, Y.; George, S. M. *J. Phys. Chem. C* **2007**, *111*, 8509.
(18) Adarnczyk, N. M.; Dameron, A. A.; George, S. M. *Langmuir* **2008**, *24*, 2081.
(19) Dameron, A. A.; Seghete, D.; Burton, B. B.; Davidson, S. D.; Cavanagh, A. S.; Bertrand, J. A.; George, S. M. *Chem. Mater.* **2008**, *20*, 3315.
(20) Jiang, Y. B.; Xomeritakis, G.; Chen, Z.; Dunphy, D.; Kissel, D. J.; Cecchi, J. L.; Brinkertt, C. J. *J. Am. Chem. Soc.* **2007**, *129*, 15446.
(21) Lee, B. H.; Ryu, M. K.; Choi, S. Y.; Lee, K. H.; Im, S.; Sung, M. M. *J. Am. Chem. Soc.* **2007**, *129*, 16034.
(22) Nilsen, O.; Klepper, K. B.; Nielsen, H.; Fjellvag, H. Organic Inorganic Hybrid Materials by ALD. In *Proceedings of the 214th ECS Meeting*; Honolulu, HI, Oct 12−17, 2008; Electrochemical Society: Pennington, NJ, 2007; abstr. 1877.

10.1021/cm8020403 CCC: $40.75
Published on Web 02/12/2009

Scheme 1[a]

$$-\mathrm{OZn(OH)(s)} + \mathrm{Zn(C_2H_5)_2} \rightarrow -\mathrm{OZn(C_2H_5)(s)} + \mathrm{C_2H_6} \quad (1)$$

$$-\mathrm{OZn(C_2H_5)(s)} + \mathrm{H_2O} \rightarrow -\mathrm{OZn(OH)(s)} + \mathrm{C_2H_6} \quad (2)$$

[a] (s) represents the surface-bonded species.

Scheme 2

$$-\mathrm{OZn(O{-}R{-}OH)(s)} + \mathrm{Zn(C_2H_5)_2} \rightarrow -\mathrm{O{-}R{-}OZn(C_2H_5)(s)} + \mathrm{C_2H_6} \quad (3)$$

$$-\mathrm{OZn(C_2H_5)(s)} + \mathrm{HO{-}R{-}OH} \rightarrow -\mathrm{OZn(O{-}R{-}OH)(s)} + \mathrm{C_2H_6} \quad (4)$$

(M−L−M) connectivity,[23] where the L denotes a functional organic ligand, commonly containing C−O units linking to the metal center. Molecular layer deposition can also result in formation of planar or three-dimensional extended inorganic hybrid materials[21] with continuous metal−oxygen−metal (M−O−M) binding units.[23] Hybrid organic−inorganic materials, however, are most widely synthesized using solution-based hydrothermal chemistry (for example, see reviews by Yaghi et al.,[24] Cheetham et al.,[23] and Rao et al.[25]). The extension into vapor-phase fabrication could open up significant new applications for hybrid materials. Vapor-phase methods, however, require precursors to be sufficiently volatile for transport without decomposition, and the reactant must provide terminal groups that enable spontaneous exothermic surface reactions.

Vapor-phase molecular layer deposition has recently been investigated to form poly (aluminum ethylene glycol) materials[19,22] of the form $(-\mathrm{O{-}Al{-}O{-}R{-}})_n$. These alkylaluminum oxide network solids are known as "alucone" polymers,[19,26,27] and were initially formed as preceramic polymers using solution-based sol−gel reaction processes. Preliminary studies of molecular layer deposition using diols and diethyl zinc have also reported formation of related "Zn−hybrid" or "zincone" polymers[28,29] of the form $(-\mathrm{O{-}Zn{-}O{-}R{-}})_n$.

The ALD process for ZnO utilizes alternating doses $\mathrm{Zn(CH_2CH_3)_2}$ and $\mathrm{H_2O}$, and previous in situ IR and QCM studies suggest it closely follows the typical ALD reaction sequence indicated in Scheme 1.[6,30,31] An analogous reaction scheme for organic−inorganic polymer MLD can be devised using a metal alkyl and a bifunctional organic monomer.[19] For example, a hypothetical scheme for reaction of diethyl zinc (DEZ) and a diol to obtain steady-state deposition of a M-L-M network $(-\mathrm{O{-}Zn{-}O{-}R{-}})_n$ zincone thin film is shown in Scheme 2. We report here an investigation of MLD surface reactions using ethylene glycol and diethyl zinc to form zincone poly (zinc ethylene glycol) hybrid organic−inorganic thin films. The growth behavior of zincone is quantified using in situ quartz crystal microbalance (QCM) and several ex situ characterization tools, and differences between growth initiation on ZnO and steady-state hybrid material deposition are observed and analyzed. The chemical and physical properties of the resulting zincone film are also of interest, including bonding structure and reactivity of the as-formed hybrid material upon exposure to ambient, and these properties are characterized by ex situ spectroscopic and imagine analysis. Transmission electron microscopy indicates that the zincone structure could be a precursor layer for fabrication of nanoporous thin films with well-controlled thickness.

2. Experimental Section

(A) ALD and MLD Precursors. Diethyl zinc ($\mathrm{Zn(C_2H_5)_2}$) (95%) was obtained from Strem Chemicals Inc. and used without further treatment. Deionized water (DI-$\mathrm{H_2O}$) was used as the water source for ZnO ALD deposition. Anhydrous ethylene glycol, EG ($\mathrm{OHC_2H_4OH}$) (99.8%) (Sigma-Aldrich) was used as the organic material source without further purification. High purity Ar (99.999%) (National Welders Supply Co.) was used as the purge gas and carrier gas for reactants.

(B) Reactor and QCM Setup for ZnO ALD and Zincone MLD. Atomic layer deposition of ZnO and molecular layer deposition of the zincone material were carried out in the same homemade viscous flow vacuum reactor. A schematic of the deposition equipment is shown in Figure 1. The reaction system is composed of stainless steel tube ~3.5 cm in diameter connected to gas inlet and pumping ports by conflat flanges. A resistively

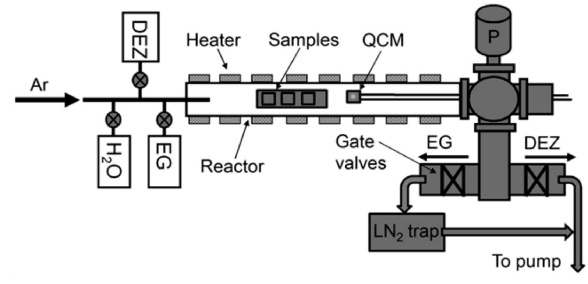

Figure 1. Schematic view of the viscous flow ALD/MLD reactor. The precursors are delivered into the reactor with Ar carrier gas. On the reactor exhaust line, computer controlled gate values are used to direct the exhaust from the EG pulse into a liquid nitrogen trap before entering the pump.

(23) Cheetham, A. K.; Rao, C. N. R.; Fellera, R. K. *Chem. Commun.* **2006**, 4780.
(24) Yaghi, O. M.; O'Keefe, M.; Ockwig, N. W.; Chae, H. K.; Eddaoudi, M.; Kim, J. *Nature* **2003**, *423*, 705.
(25) Rao, C. N. R.; Cheetham, A. K.; Thirumurugan, A. *Journal of Physics: Condensed Matter* **2008**, *20*, 083202.
(26) Rees, W. S.; Hesse, W. Preceramic Polymers for Aluminum Oxide. In *Chemical Perspectives of Microelectronic Materials II*; Iterrante, L. V., Jensen, K. F., Dubois, L. H., Gross, M. E., Eds.; Materials Research Society: Pittsburgh, PA, 1991; Vol. 204, p 563.
(27) McMahon, C. N.; Alemany, L.; Callender, R. L.; Bott, S. G.; Barron, A. R. *Chem. Mater.* **1999**, *11*, 3181.
(28) Peng, Q.; VanGundy, R. M.; Hyde, G. K.; Parsons, G. N. Atomic Layer Deposition of Zinc Oxide/Organic Hybrid Material from Diethyl Zinc and Ethylene Glycol. In *2008 AVS International Topical Conference on Atomic Layer Deposition (ALD2008)*; Bruges, Belgium, June 29−July 2, 2008; AVS, Chico CA, 2008.
(29) Yoon, B.; O'Patchen, J. L.; Davidson, S. D.; Segheste, D.; Cavanagh, A. S.; George, S. M. Molecular Layer Deposition of Hybrid Organic-Inorganic Polymers Based on Metal Alkyl and Diol Reactants.In *2008 AVS International Topical Conference on Atomic Layer Deposition (ALD2008)*Bruges, Belgium, June 29−July 2, 2008; AVS, Chico CA, 2008.
(30) Yousfi, E. B.; Fouache, J.; Lincot, D. *Appl. Surf. Sci.* **2000**, *153*, 223.
(31) Ferguson, J. D.; Weimer, A. W.; George, S. M. *J. Vac. Sci. Technol., A* **2005**, *23*, 118.

heated jacket surrounding the system is used to achieve the desired temperature. A controlled temperature gradient was maintained along the entire gas flow path to prevent precursor condensation. Ultra-high-purity Ar gas was used as the carrier gas and further purified by using a gas filter (DRIERITE Gas Purifier) before entering the reaction system.

For a typical ZnO deposition cycle, the gas exposure time for the DEZ and H_2O was 2 and 4 s, respectively, with an Ar purge time of 42 s between each reactant pulse. This process cycle is denoted as DEZ/Ar/H_2O/Ar = 2/42/4/42 s. The flow rate of Ar carrier gas is ~120 standard cubic centimeters per minute (sccm) with a steady-state process pressure of ~0.9 Torr monitored by a Baratron pressure gauge (MKS Instrument Inc.). The reaction system was pumped using a rotary mechanical pump. As shown in the reactor schematic in Figure 1, the gas effluent during the EG or H_2O cycle was directed through a liquid nitrogen trap to eliminate reaction with excess DEZ in the pump. The sample substrates and the QCM crystal were heated by convection and radiation from the heated reactor wall. The substrate samples were silicon wafer pieces, prepared by wet cleaning in BakerClean JTB-100 solution (Mallinckrodt Baker Inc.), followed by rinsing in DIH_2O and blown-dry with N_2, which results in a thin chemical oxide surface. Sample substrates were fixed onto an aluminum sample boat before loading into the reaction chamber. The in situ QCM was installed onto the deposition reactor system through the inlet of the reactor as show in Figure 1. Polished QCM crystal sensors with Au coating (Colorado Crystal Corp.) were mounted in the Maxtek BSH-150 bakeable sensor head. The sensor head was modified to allow ~10 sccm of Ar flow over the back side of the sensor, and the crystal was sealed to the QCM housing using conductive epoxy to prevents material from depositing onto the backside of the crystal surface.[32] The mass change signals were detected by a monitor (Maxtek TM-400), and recorded using a home designed LABVIEW program.

(C) Precursor Delivery System. The DEZ precursor was stored in a stainless steel bottle and evaporated at room temperature (~25 °C). The DI-H_2O and EG were also stored in stainless steel containers and evaporated at room temperature and 80 °C, respectively. The DI-H_2O and DEZ vapors were bled into the reactor using Ar carrier gas through a computer-controlled ALD solenoid valve in series with a needle valve. The amplitude of the pressure increase during the DEZ and H_2O pulses is ~50 mTorr. The EG container was connected to the system using only a solenoid valve, and the pressure increase during EG dose is also ~50 mTorr. The reactant dose amount was adjusted by either changing pulse time or by changing the flow through the needle valve orifice. The organic and metal organic precursors were pumped through separate exhaust lines, which were controlled separately using computer-controlled gate valves. As illustrated by the schematic in Figure 1, the reactor was designed to allow simple transitions between deposition of ZnO ALD and MLD of zincone materials by switching easily between H_2O and EG reactant flow.

(D) Ex situ Film Characterization. The composition of synthesized material was analyzed using transmission Fourier transform infrared spectroscopy (FTIR). A ThermoNicolet IR bench with a deuterated triglycine sulfate detector (KBr bean splitter) was used in the transmission mode with 2048 scans at 4 cm^{-1} resolution. The measuring chamber was continuously purged with purified dry air (ambient without water moisture). A background spectrum was collected using the starting Si wafer before the deposition. X-ray photoelectron spectroscopy (XPS) analysis was performed with a Kratos Analytical Axis Ultra equipment with a monochromatic Al Kα source operated at 15kV. For all samples, the C 1s peak ($-C-H_2$) was normalized to 284.6 eV as the reference. For the survey and detail scans, 160 and 20 were used for the pass energy, respectively. Before spectrum collection, the sample surfaces were cleaned in situ with 3 min of Ar sputtering at 5 kV.

Surface morphology of films was analyzed by a Nanoscope IIIa atomic force microscope (Digital Instruments) operated in tapping mode with a scanning frequency of 0.5 Hz. X-ray diffraction spectra were obtained using a Bruker AXS D-5000 X-ray diffractometer equipped with GADDS area detector. All measurements were taken by using a generator with a voltage of 40 kV and a current of 30 mA.

Film thickness and refractive index were measured using variable-angle spectroscopic ellipsometry (J. A. Woollam). Measurement was carried out over a spectrum from 400 to 1100 nm using incident angles of 65, 70, and 75°. A three-layer Cauchy model (hybrid/nativeSiO_2/Si) was used to fit the experiment data to derive the refractive index and film thickness. In the model, thickness of native oxide and Si substrate were set at 15 Å and 1 mm, respectively.

The deposited Zn−hybrid material was also examined by transmission electron microscopy (TEM). For this analysis, TEM grids (Ted Pella, Inc.) were loaded with Al_2O_3 microtubes fabricated by ALD, and then used as the substrate for the zincone deposition. For this process, Al_2O_3 microtubes were fabricated by coating a polyvinyl alcohol (PVA) electrospun fiber template with 500 cycles Al_2O_3 ALD at 45 °C, followed by calcination in ambient at 400 °C for 24 h to remove the PVA.[11] The as-formed Al_2O_3 microtubes were dispersed in ethanol and sonicated for 1 min. Several droplets of the dispersion solution were pipetted onto the carbon film coated TEM grid, and grids were dried at room temperature overnight, and then heated to the reaction temperature in vacuum for 1 h before being exposed to the MLD deposition process. The samples were removed from the reactor and imaged with an FEI Tecnai G^2 Twin microscope operated at 160 kV. All samples were exposed to ambient for more than 12 h before TEM analysis.

3. Experimental Results

(A) In situ QCM Analysis of ZnO ALD. In situ quartz crystal microbalance results obtained during ZnO ALD are shown in Figures 2 and 3. Figure 2a shows the mass uptake data from ZnO ALD using DEZ/Ar/H_2O/Ar = 2/42/4/42 s at 120 °C over a large number of cycles on the gold-coated quartz crystal. The ZnO film growth is linear with the number of deposition cycles, with an average mass gain of about 125 ± 3 ng/(cm^2•cycle), where the error reflects the standard deviation. Ellipsometry analysis of deposited films indicates a growth rate of ~2.25 Å/cycle at 120 °C for deposition up to 1000 ALD cycles, consistent with literature reports of 120−140 ng/(cm^2•cycle) and 2.1−2.8 Å/cycle,[6,30] respectively, for ZnO ALD. Moreover, the film density estimated from the mass uptake rate and growth rate is (125 ng/cm^2•cycle)/(0.225nm/cycle) ≈ 5.56 g/cm^3, in good agreement with the literature value[6,30] of 5.61 g/cm^3.

A detailed view of QCM results obtained during ZnO ALD at 120 °C is shown in Figure 2b, where the dashed regions refer to the reactant pulsing steps. The QCM results display a large mass uptake of ~125 ng/(cm^2•cycle) during the DEZ exposure and a small mass loss of ~ 3 ng/(cm^2•cycle) upon reaction with H_2O, consistent with previous QCM analyses of ZnO ALD.[6,30] Note that when the DEZ exposure is repeated without a H_2O step, a much smaller mass uptake

(32) Elam, J. W.; Groner, M. D.; George, S. M. *Rev. Sci. Instrum.* **2002**, *73*, 2981.

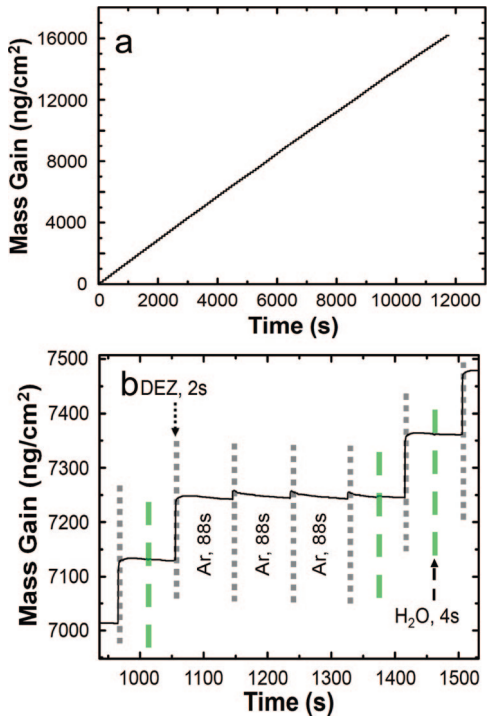

Figure 2. (a, b) In situ QCM results for ZnO ALD at 120 °C using DEZ/Ar/H_2O/Ar exposure times of 2/42/4/42 s. Panel (a) shows linear mass gain for more than 130 ALD cycles. The average mass uptake rate is ~125 ng/(cm^2·cycle) with standard deviation of 3 ng/(cm^2 cycle). Panel (b) shows an interrupted ZnO ALD sequence at 120 °C, showing the effect of three sequential DEZ/Ar (2/88 s) ALD half-cycle exposures. The DEZ dose time is indicated by the dotted line, and the H_2O dose is indicated by the dashed line. Repeating the DEZ exposure results in a small mass uptake, followed by a slow mass decrease, consistent with some reactant physisorption.

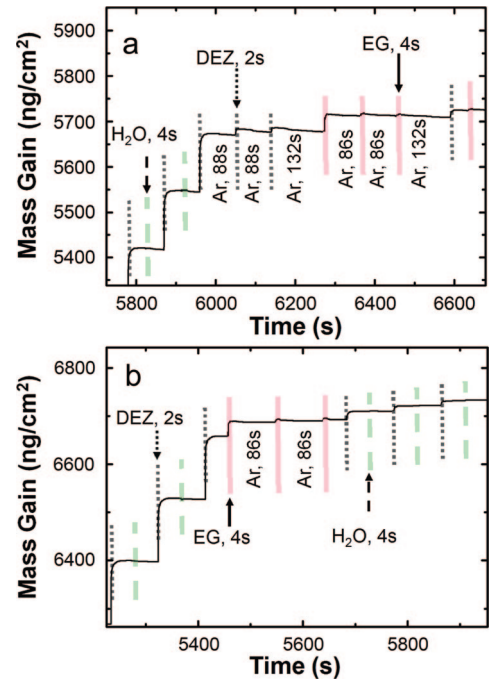

Figure 3. In situ QCM results at 120 °C showing the effect of EG exposure on the $-OZn(C_2H_5)_{(s)}$ saturated surface produced during ZnO ALD. Two data sets are shown from two separate experiments. The DEZ dose is indicated by the dotted line, and the H_2O dose is indicated by the dashed line. The EG dose is shown with the shaded solid line. The first EG exposure result in mass uptake and surface saturation. The EG exposure results in significantly decreased mass uptake for subsequent DEZ exposure steps.

of ~15 ng/(cm^2·cycle) is followed by a slow mass decrease during subsequent Ar purge, concluding with virtually no net mass uptake. This result is consistent with a chemically saturated $-OZn(C_2H_5)$(s) surface after one pulse 4 s DEZ exposure. The QCM data also show that after the three DEZ exposure steps on the saturated $-OZn(C_2H_5)$(s) surface, the regular ZnO ALD growth can be readily restarted with the same mass uptake per cycle as the steady-state growth by exposing the saturated surface to H_2O/Ar/DEZ/Ar cycles.

(B) Ethylene Glycol Adsorption on the ALD ZnO Surface. Vapor-phase ethylene glycol was used in place of water in the ZnO ALD reaction sequence, and QCM was used to monitor the mass changes and surface saturation. These studies have two points of interest. First, it is important to determine to what extent EG can react with the surface-bonded $-OZn(C_2H_5)$(s) ligands, on the ZnO ALD substrate. Second, it is important to characterize the extent to which DEZ can react with the surface bonded $-Zn(OC_2H_4OH)$(s) ligands generated during the EG exposure. Although the QCM results may not confirm the detailed surface reaction stoichiometry implied in the given Schemes, QCM will allow quantitative analysis of the relative mass uptake during surface exposure sequences. Specifically, after confirming steady-state ALD growth of ZnO on the QCM crystal, the $-OZn(C_2H_5)$(s) ligand saturated ALD ZnO surface was exposed to EG molecules and the mass gain was monitored by QCM. Data in Figure 3a initially shows two full cycles of DEZ/Ar/H_2O/Ar, with average mass uptake of ~127 ng/(cm^2·cycle), which agrees well with the results shown in Figure 2. The first two DEZ/H_2O cycles are followed by two Ar/DEZ cycles (88/2 s) and a longer (132 s) Ar exposure, then this surface is exposed to three ethylene glycol vapor pulses of 4 s each. The two Ar/DEZ exposure steps again show evidence for surface saturation, consistent with formation of a -$OZn(C_2H_5)_{(s)}$ saturated ALD ZnO surface. Upon exposing the $-OZn(C_2H_5)$(s) saturated ZnO surface to EG (near $t \approx 6280$ s in Figure 3a), the QCM results show a mass uptake of ~33 ng/cm^2. The next two EG/Ar exposure steps show some evidence for physisorption, but no net mass gain, consistent with surface saturation. This surface was then exposed to DEZ for 2 s (near $t = 6600$ s), and the mass uptake was ~16 ng/cm^2. After the DEZ exposure and Ar purge steps, exposure to EG results in a mass uptake of ~3 ng/cm^2, which is also less than that observed for the first EG exposure on the $-OZn(C_2H_5)$(s) saturated ZnO surface.

Figure 3b shows another set of representative QCM results similar to Figure 3a, where the $-OZn(C_2H_5)$(s) terminated ALD ZnO surface is exposed to three EG/Ar exposure cycles at 120 °C. This second set of data collected separately from that in Figure 3a, is included in part to demonstrate the reproducibility of the data collection. The first EG/Ar exposure (near $t = 5470$ s) results in a net mass uptake of ~34 ng/cm^2, similar to the 33 ng/cm^2 observed in Figure 3a. Again, exposing this surface to additional pulses EG resulted in virtually no net mass uptake, consistent with a reaction-saturated surface. The three short EG exposures are followed by three DEZ/Ar/H_2O/Ar cycles (starting at $t \approx$

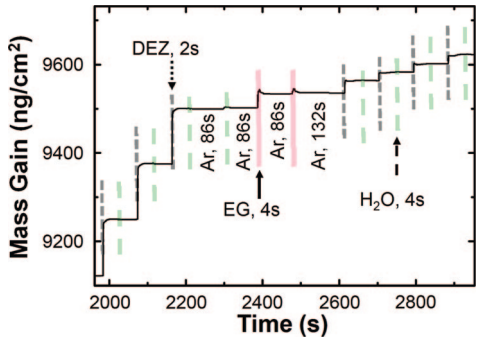

Figure 4. In situ QCM results at 120 °C showing the effect of EG exposure on the $-OZn(OH)_{(s)}$ saturated surface produced during ZnO ALD. The DEZ dose is indicated by the dotted line, and the H_2O dose is indicated by the dashed line. The EG dose is shown with the shaded solid line. Exposing the −OH terminate surface to EG results in a mass uptake of ∼33 ng/cm^2.

Scheme 3

$$-OZn(OH)(s) + OHC_2H_4OH \rightarrow -OZn(OC_2H_4OH)(s) + H_2O \quad (5)$$

5690 s). The overall mass uptake during the first three ZnO ALD cycles on the EG-exposed surface is significantly reduced as compared to steady-state ZnO ALD. Further QCM analysis indicates that continuing the DEZ/Ar/H_2O/Ar exposure sequence results in a slow increase in mass uptake per cycle, returning to the full steady-state ZnO growth rate after ∼40 cycles. Results in panels a and b in Figure 3 also show that when the ALD ZnO surface is exposed to EG (after the DEZ exposure half-cycle) the mass uptake is larger than that observed during steady-state Zincone MLD. The same result was observed at other temperatures studied.

One may expect that because the saturated $-OZn(OH)_{(s)}$ surface generated during ZnO ALD is not reactive to further H_2O exposure, it will also not be reactive with EG. Figure 4 shows QCM results where a $-OZn(OH)(s)$ terminated surface formed during steady-state ZnO ALD was exposed to H_2O/Ar (2/86 s) exposure (at $t \approx 2310$ in Figure 4), followed by EG exposure and Ar purge. As expected, the second sequential H_2O exposure resulted in no mass uptake. However, the first EG exposure results in a net mass gain of ∼33 ng/cm^2, and this mass increase is stable during an extended Ar purge. A subsequent EG/Ar exposure resulted in no observed mass gain, consistent with a saturated surface. The mass uptake during EG exposure is attributed to the dehydration reaction shown in Scheme 3, where the surface Zn-OH reacts with vapor-phase HO-(C_2H_4)-OH to produce Zn−O-(C_2H_4)-OH + H_2O.[33] Further insight into surface reactions can be gained by analysis of steady-state Zn-hybrid growth.

(C) QCM Analysis of Steady-State Zn−Hybrid MLD. Steady-state MLD growth of Zn−hybrid films was analyzed by QCM, and representative results are shown in Figure 5. The average net mass uptake during the DEZ and EG pulse, measured during the purge cycle after stabilization, is ∼20.4 ± 1.3 ng/(cm^2·cycle) and ∼4.8 ± 1.4 ng/(cm^2·cycle), respectively. The uncertainty values represent the standard deviation of more than 50 mass uptake values measured during steady-state deposition, and is ascribed to the mass resolution in the QCM, as well as small variations in flow or temperature during processing.

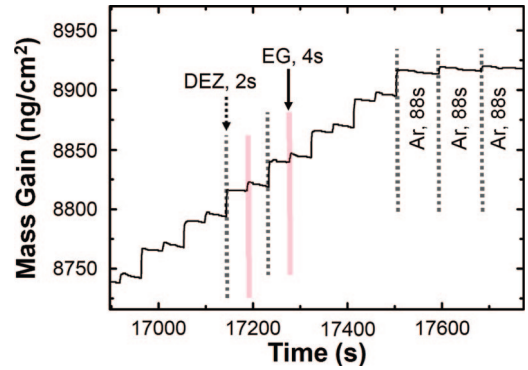

Figure 5. In situ QCM results at 120 °C during steady-state molecular layer deposition. The DEZ dose is indicated by the dotted line, and the EG dose is shown with the shaded solid line. After an EG/Ar half-cycle, the DEZ/Ar (2/88 s) half-cycle was repeated 3 times, resulting in mass uptake followed by approximately equivalent mass loss, indicative of DEZ physisorption/desorption.

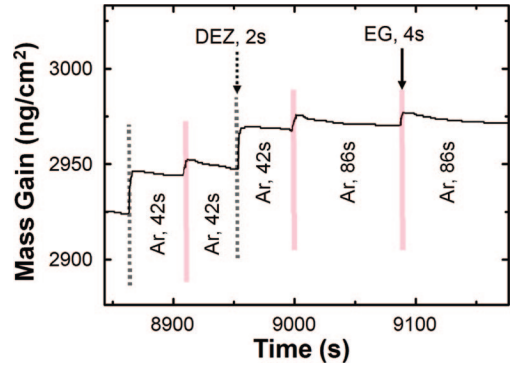

Figure 6. In situ QCM results at 120 °C during steady-state molecular layer deposition using the same conditions shown in Figure 5. After a DEZ/Ar half-cycle, the EG/Ar (4/86 s) half-cycle was repeated 2 times, resulting in mass uptake followed by approximately equivalent mass loss, indicative of reactant physisorption/desorption. No net mass gain is observed during the repeated EG/Ar half-cycles.

Following many cycles of steady-state growth, the surface generated during EG/Ar (2/42 s) half-cycle, is exposed to three DEZ/Ar half-cycles (2/88 s). Repeating the DEZ exposure (at $t \approx 17600$ and 17700 s in Figure 5) results in mass uptake, followed by a slow decrease, with no net mass increase obtained. The slow mass decrease during the purge step following the DEZ exposure is consistent with physisorption of DEZ on the growth surface, or diffusion into the near-surface region of the growing film.[19] Results in Figure 5 indicate that one 2 s DEZ exposure during steady-state growth is sufficient for surface saturation in the MLD process.

The data in Figure 6 examine more closely the surface saturation after EG exposure during steady-state growth. The figure shows one full DEZ/Ar/EG/Ar (4/42/4/42) cycle ($t \approx$

(33) Hausmann, D.; Becker, J.; Wang, S. L.; Gordon, R. G. *Science* **2002**, *298*, 402.

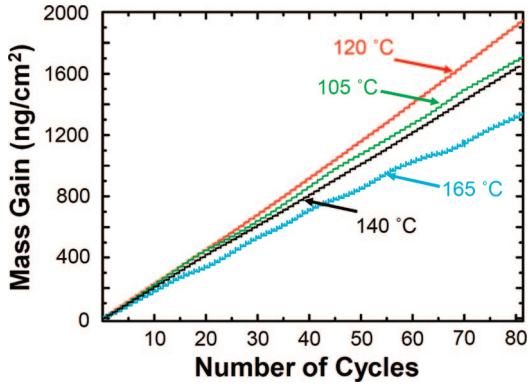

Figure 7. In situ QCM results at various temperatures during steady-state molecular layer deposition using DEZ/Ar/EG/Ar: 2/42/4/42 s. The mass uptake rate decreased with increasing temperature, resulting in an average mass uptake of ~24.3 ng/(cm^2·cycle) at 120 °C and ~17.4 ng/(cm^2 cycle) at 165 °C. Data were not collected during film nucleation, so data from an arbitrary starting time were normalized to the origin.

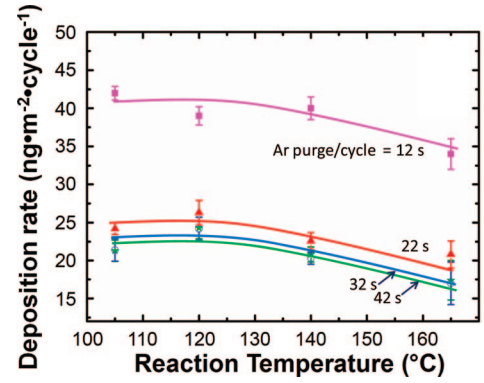

Figure 8. Plot of the net mass uptake rate versus deposition temperature for various Ar purge times: DEZ/Ar/EG/Ar = 2/*n*/4/*n* s, where *n* is 12, 22, 32, or 42 s. The mass uptake rate of Zn hybrid MLD decreases with increasing purge time and reaction temperature. The error bars were deduced from the corresponding QCM measurements, and the lines are a guide for the eye. The data at 32 and 42 s are statistically indistinguishable for all studied temperatures.

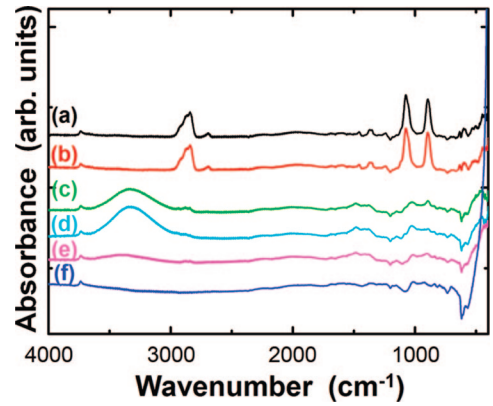

Figure 9. FTIR spectra collected from an example Zn−hybrid MLD film deposited using 800 cycles at 120 °C: (a) after immediate transfer to dry air; (b) in dry air for 3 days; (c) after exposure to ambient for 1 h; (d) after ~12 h at ambient; and (e) after annealing at ambient at 100 °C for ~2 h. Spectrum (f) is obtained from an ~45 nm thick ALD ZnO film deposited using 200 cycles at 120 °C.

8870−8906 s), followed by another similar cycle with a longer 86 s Ar purge after the EG exposure (between $t \approx$ 8960 and $t \approx$ 9090 s). The EG exposure is estimated to be ~100 mTorr s during the 4 s EG pulse step. The QCM generally shows initial mass gain, followed by a slower mass loss, with a net mass uptake of ~3.5 ng/(cm^2·cycle) after the 42 s purge. The cycle with the longer Ar purge generally shows a similar net mass uptake within the uncertainty of QCM measurement. When the EG/Ar (4/86 s) cycle was repeated (between $t \approx$ 9090 and 9180 s), the QCM showed adsorption and desorption with nearly no net mass uptake. The effect of purge time and temperature on the surface saturation is quantified in more detail below.

In situ QCM results obtained over many cycles at several deposition temperatures during steady-state Zn−hybrid film growth are shown in Figure 7. The deposition rate decreases slightly with increasing deposition temperature, and overall average mass uptake rate decreased from ~24.3 ± 1.4 ng/(cm^2·cycle) to ~17.4 ± 2.8 ng/(cm^2 cycle) as the reaction temperature increased from 120 to 165 °C. The data collected at 165 °C shows some variation of the mass uptake rate during the deposition, which may be due to small temperature fluctuations during the QCM measurement.[34] The decrease in film growth rate with increasing temperature indicates kinetically controlled surface reactions during the hybrid MLD deposition,[30] including for example an enhanced rate of precursor desorption with increasing temperature.[16] Dameron et al.[19] found that during alucone MLD, film deposition rate decreased with increasing temperature, except during the first 2−5 alucone MLD cycles on Al_2O_3 where the rate was nearly independent of temperature. For our studies, data was not collected during film nucleation, and Figure 7 shows data normalized to the origin from an arbitrary starting time.

To further analyze the effect of precursor adsorption, the effect of gas purge time on the overall mass uptake rate was analyzed using in situ QCM at temperatures between 105 and 165 °C, and results are summarized in Figure 8. Increasing the Ar purge time after DEZ and EG pulses from 12 to 42 s resulted in a decrease in net mass uptake rate, consistent with removal of physisorbed reactants. No significant difference is observed by extending purge times from 32 to 42 s, which is in agreement with surface saturation and self-limiting MLD type growth. In order to ensure consistent self-limiting MLD, the 42 s purge time was used to obtain the films used for characterization discussed below.

(D) FTIR Results and Stability of Zn−Hybrid Films. Chemical composition and bonding in the Zn−hybrid films after deposition were examined using FTIR. Generally, the films were observed to be sensitive to ambient laboratory air, and the film thickness decreased upon exposure to ambient, as discussed below. For IR analysis, as-formed zincone films were transferred immediately from the reactor into the dry air-purged analysis chamber. Characterization of Zn-hybrid films with short (<2 min) and long (several hours) exposures to ambient was performed in order to illustrate the instability mechanisms of the Zn−hybrid materials. Figure 9 shows representative FTIR spectra of a Zn−hybrid film deposited with 800 cycles at 120 °C: (a) in dry air for 1 min; (b) in dry air for 3 days; (c) in ambient for 1 h; (d) in ambient for 12 h; and (e) after further annealing in ambient at 100 °C for 2 h. For reference, spectrum (f) in Figure 9 shows IR absorbance for an ~45 nm ZnO ALD film deposited at 120 °C for 200 cycles. The as-deposited

Zn−hybrid film in spectra (a) and (b) shows peaks primarily in the range of 2600−3000 and 800−1600 cm^{-1}. The modes at 2921, 2868, 2840, and 2690 cm^{-1} are ascribed to antisymmetric, symmetric, and combination C−H modes in $-CH_2-$ units.[19,35–39] Similar differentiation of $-CH_2-$ IR modes in ethylene glycol is observed upon covalent grafting, depending on the chemical environment of the surface-bound ligand.[38] The relatively small peaks at 1462, 1454, 1370, 1353, and 1240 cm^{-1} are ascribed to $-CH_2-$ scissor, twist, and wag modes.[19,35–39] Peaks at 1181 and 1145 cm^{-1} are related to C−C stretch, and the large peak at 1075 cm^{-1}, and the shoulder at 1053 cm^{-1}, are ascribed to C−O vibrations in C−C−O and Zn−O−C bonding units. The peak at 895 cm^{-1} is associated with combined $-CH_2-$ vibrations. These IR peaks confirm the successful covalent incorporation of ethylene glycol to form the metal-organic hybrid thin film polymer $(-O-Zn-O-C_2H_4-)_n$. No detectable characteristic peaks from other organic components were found in the FTIR spectra of the as-formed Zn−hybrid materials.

Spectrum (b) in Figure 9 was obtained after storing the sample for several days in dry air in the FTIR analysis chamber. The IR absorbance appears the same as the as-deposited film, indicating good stability in dry air. However, exposure to relatively humid laboratory air for 1 h resulted in significant change of the IR spectrum, as shown in spectrum (c). The C−H stretching and deformation modes of $-CH_2-$ are significantly reduced, and the features associated with C−O modes become nearly indiscernible, indicating significant reaction, likely with water in the ambient. Significant −OH bonding appears near ∼3300 cm^{-1}, consistent with water vapor inserting into the ethoxy linkage and releasing volatile glycol species. Ambient exposure also results in a decrease in total film thickness, consistent with material volatilization and visible color change. The metal M−O−R bonding in the zincone material (where R is the organic ligand) is generally unstable. The Si−O−C bonding in 3-aminopropyltriethoxysilane or other ethoxylsilanes or methoxysilanes, as well as bonds in Zn methoxyethoxide, are readily hydrolyzed by moisture from the ambient. Extended ambient exposures up to 12 h resulted in no further significant change in the IR spectrum, as shown in spectrum (d) in Figure 9, indicating the reaction between the Zn−hybrid film and moisture from ambient proceeded relatively quickly. Similar instability was observed for zincone films deposited at other temperatures, and it has also been reported for alucone films deposited by MLD.[19] Ambient-exposed samples were also annealed in ambient at temperatures up to 100 °C. As shown in spectrum (e), annealing at 100 °C for 2 h resulted in a decrease in hydroxide bonding and an increase in features related to Zn−O bonding near 400 cm^{-1}, consistent with a structure similar to that observed for the ALD ZnO shown in spectrum (f). In the discussion below, the resulting films after ambient exposure are referred to as "hydrolyzed Zn−hybrid" material.

(E) Thickness Dependence of FTIR and Ellipsometry Results. Figure 10 shows FTIR spectra of Zn-hybrid films with different thicknesses deposited at 120 °C. The characteristic IR peaks associated with C−H and C−O modes in ethylene oxide are observed to increase with the number of deposition reaction cycles, consistent with the QCM data shown in Figures 5−7. As mentioned above, the film thickness was observed to be unstable with time. To observe the thickness change, part of a freshly deposited ZnO−hybrid film was covered with a glass slide and the sample left in laboratory air overnight. The uncovered film visibly changed, and step profilometry confirmed that the thickness of the exposed film had decreased. Similar measurements on other samples indicated that the film reacted with moisture within 1−2 h upon ambient exposure. Because of this instability, reliable thickness measurements of as-deposited films were difficult to obtain. However, thickness values obtained from spectroscopic ellipsometry analysis of fully hydrolyzed

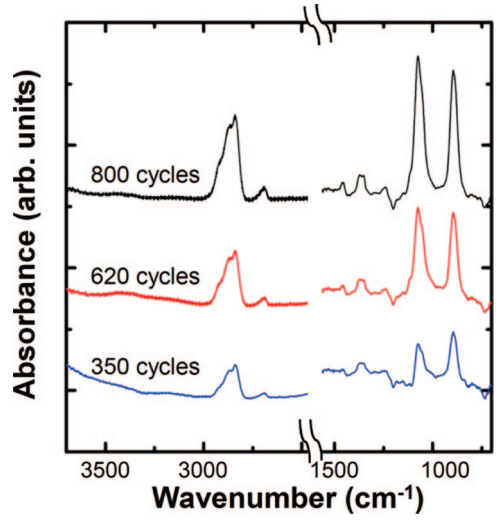

Figure 10. FTIR spectra obtained from three Zn−hybrid MLD films deposited at 120 °C using different numbers of MLD cycles. All samples received a similar brief ambient exposure before analysis. The intensity of the characteristic EG peaks increase with the number of deposition cycles.

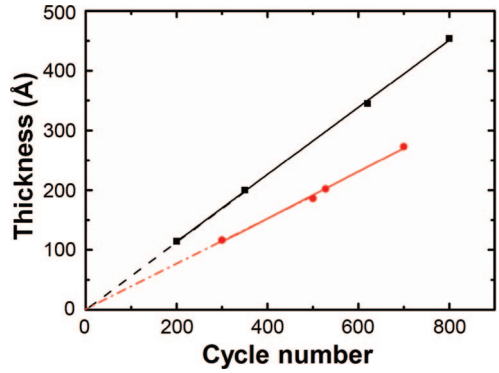

Figure 11. Film thickness of hydrolyzed Zn−hybrid films obtained from spectroscopic ellipsometry, plotted versus number of MLD cycles for films deposited on oxidized silicon. The typical uncertainty in each measurement is ∼1−2%. The solid lines give linear fits corresponding to a deposition rate of 0.57 Å/cycle at 120 °C (■) and 0.39 Å/cycle at 165 °C (•).

(34) Rocklein, M. N.; George, S. M. *Anal. Chem.* **2003**, *75*, 4975.
(35) Harder, P.; Grunze, M.; Dahint, R.; Whitesides, G. M.; Laibinis, P. E. *J. Phys. Chem. B* **1998**, *102*, 426.
(36) Aranda, P.; Ruiz-Hitzky, E. *Appl. Clay Sci.* **1999**, *15*, 119.
(37) Tunney, J. J.; Detellier, C. *Clays Clay Miner.* **1994**, *42*, 552.
(38) Guimaraes, J. L.; Marangoni, R.; Ramos, L. P.; Wypych, F. *J. Colloid Interface Sci.* **2000**, *227*, 445.
(39) Wypych, F.; Schreiner, W. H.; Marangoni, R. *J. Colloid Interface Sci.* **2002**, *253*, 180.

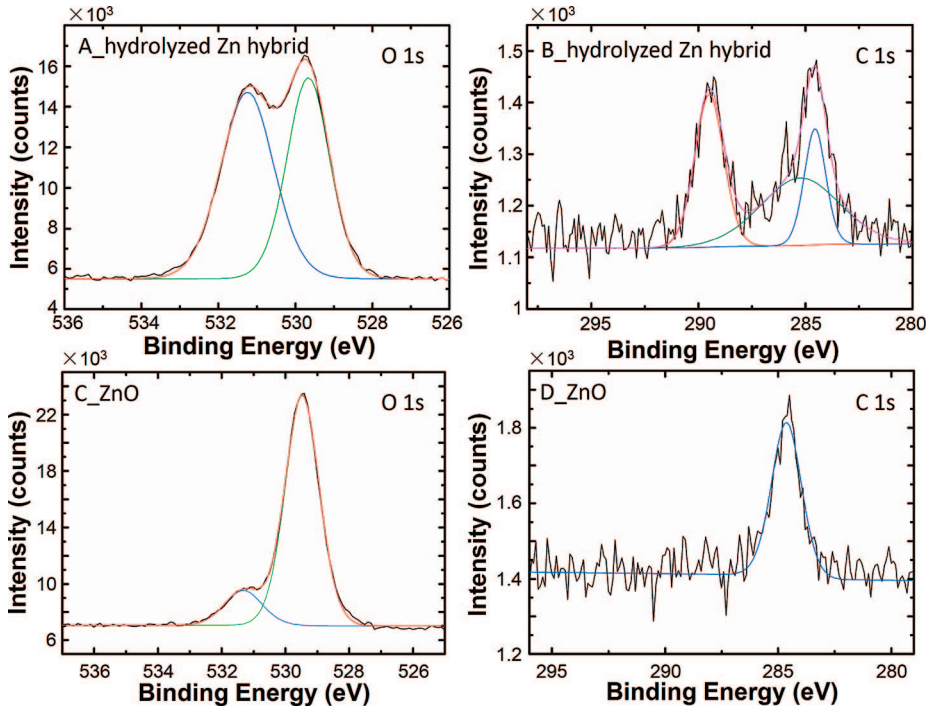

Figure 12. (a, b) O1s and C1s XPS spectra collected from a hydrolyzed MLD Zn−hybrid film (∼45 nm, 800 cycles, at 120 °C). The O1s signal shows features at 531.5 and 529.7 eV corresponding to zinc hydroxide (54.5%) and zinc oxide (45.5%), respectively. The C1s signal includes components 284.6, 285.7, and 289.4 eV related to $-C-H_2$, $-C-OH$ and $-O-C=O$, respectively. (c, d) O1s and C1s XPS spectra collected from an ALD ZnO film (∼45 nm, 200 cycles, at 120 °C). The carbon content is ∼2 at %. Ar sputtering (5 KeV for 3 min) was used to remove surface contamination before spectra collection. Gaussian curve fits are included.

Zn−hybrid films, shown in Figure 11, indicate that the thickness increased linearly with the number of deposition cycle, with a deposition rate of ∼0.57 Å/cycle at 120 °C and ∼0.39 Å/cycle at 165 °C. The spectroscopic ellipsometry measurement data can be readily fit with the three-layer Cauchy model using a refractive index of 1.55 ± 0.05 for the hydrolyzed Zn−hybrid film.

(F) X-Ray Photoelectron Spectroscopy of Hydrolyzed Zn−Hybrid Films. Typical ALD ZnO and fully hydrolyzed Zn−hybrid films were characterized using X-ray photoelectron spectroscopy. The transfer of samples from the reactor to the XPS chamber precluded analysis of materials before ambient exposure. Survey scans of the hydrolyzed Zn−hybrid material show features similar to the control ZnO ALD film. High resolution scans of the O 1s and C 1s spectra for a hydrolyzed Zn-hybrid film (800 DEZ/EG cycles at 120 °C, ∼45nm) are shown in Figure 12a and b (top panels). Results obtained from an ALD ZnO film (200 DEZ/H_2O cycles at 120 °C, ∼45 nm) are shown in panels c and d in Figure 12 (bottom panels). The O 1s spectrum of the hydrolyzed Zn−hybrid film shows peaks at 531.5 eV corresponding to Zn−hydroxide, and at 529.7 eV related to Zn−O bonding, consistent with the IR results. The integrated intensity of the Zn−OH and Zn−O modes indicate that nearly 55% of the O is bound as Zn−OH. The hydrolyzed Zn−hybrid shows peaks at 284.6, 285.7, and 289.4 eV in the C 1s spectrum corresponding to $-C-H_2$, $-C-OH$, and $-O-C=O$, respectively, likely due to residue from EG species. The carbon content in the hydrolyzed Zn−hybrid film estimated from XPS is ∼5.6 at %. The spectra from the ALD ZnO film in panels (c) and (d) show a significantly smaller hydroxide and $C-H_2$ peaks, corresponding to <2 at % carbon, with negligible $-C-OH$ and $-O-C=O$ bonding.

(G) Surface Morphology and X-ray Diffraction of Hydrolyzed and Annealed Zn−Hybrid Films. The surface morphology of hydrolyzed Zn−hybrid thin films were characterized using scanning probe microscopy, and a representative image of a film deposited using 800 cycles at 120 °C with thickness of 45 nm is shown in Figure 13a. The overall root-mean-square (rms) roughness of the hydrolyzed Zn−hybrid film is ∼0.8 nm. Features consistent with holes in the film with average diameter ∼20−30 nm are observed, with excess material present at the edge of the features. These hole structures likely formed during postdeposition reaction with the ambient. Upon annealing at 100 °C in air for 2 h, the thickness of the hydrolyzed films decreased from ∼45 to ∼30 nm as measured by ellipsometry, and the roughness increased to 1.4 nm. It is interesting to note that the morphology becomes less well discerned after the thermal annealing process as shown by the scanning probe image in Figure 13b. X-ray diffraction results of the ZnO films deposited at 140 °C show the characteristic 100 and 002 diffraction peaks of ZnO. An organic−inorganic hybrid film deposited at 140 °C and measured after air exposure shows only broad features, characteristic of an X-ray amorphous structure.

(H) Transmission Electron Microscopy of Hydrolyzed Zn−Hybrid Films. Zn−hybrid film samples for transmission electron microscopy were prepared by performing Zn−hybrid MLD onto Al_2O_3 microtubes. The microtubes were formed using 500 ALD cycles of Al_2O_3 onto polyvinyl alcohol fibers, followed by calcination.[11] The microtubes were then mounted

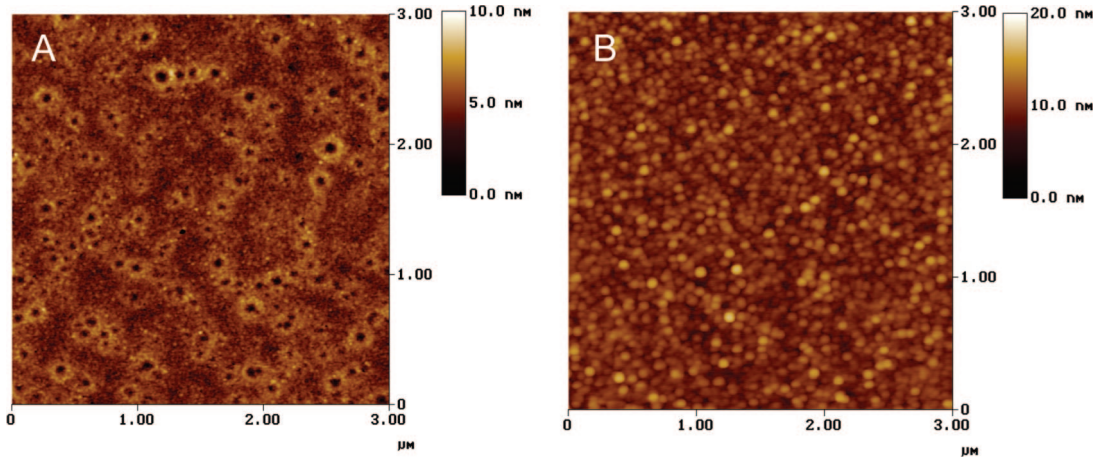

Figure 13. (a) Scanning force micrograph of a MLD Zn−hybrid film deposited at 120 °C for 800 cycles after prolonged air exposure. The film thickness is ∼45 nm and root-mean-square (rms) roughness is 0.8 nm. The surface features with diameter of 20−30 nm are cavities or holes in the film. (b) Acquired after annealing the film in image (a) in ambient for 2 h at 100 °C. The film thickness decreased to ∼30 nm and rms increased to 1.4 nm. The surface appears more homogeneous without obvious voids or holes at the scale imaged.

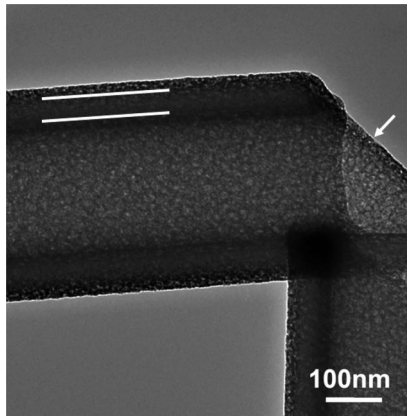

Figure 14. Transmission electron micrograph obtained from a hydrolyzed Zn−hybrid film deposited at 165 °C for 528 cycles onto two Al_2O_3 microtubes. The white lines depict the outline of the starting Al_2O_3 shell, and the right side of the image shows a region where the tube is broken allowing plan-view through the Zn−hybrid/Al_2O_3/Zn−hybrid laminate. The hydrolyzed Zn−hybrid MLD film is conformal and uniform with thickness ∼20 nm. The white arrow indicates a point with high contrast, suggesting through-holes present in the hydrolyzed film.

on TEM grids and exposed to the Zn−hybrid MLD process for 528 cycles at 165 °C. The resulting coated tubes were open to ambient at room temperature for more than 12 h before TEM imaging. A representative TEM image is shown in Figure 14. The image shows two coated tubes oriented approximately perpendicular to each other. The cross-sectional view of the horizontal hollow tube (toward the left side of the image) shows a 42 nm Al_2O_3 shell (denoted by the white lines) surrounded by ∼20 nm of hydrolyzed Zn-hybrid coating on the inside and outside of the tube. The outer coating is most easily discerned because of better electron contrast when imaging through only the single film layer. The film thickness obtained from the image of the outer layer agrees well with the thickness values of similar films deposited on planar Si wafers and measured by spectroscopic ellipsometry. The horizontal tube is broken revealing a region (toward the right side of the image) allowing a plan-view image of the Zn−hybrid/Al_2O_3/Zn−hybrid structure, showing nonuniform electron contrast. The TEM image shows that the hydrolyzed Zn−hybrid coating is uniform and conformal on both the inner and outer surfaces of the microtube. The contrast observed in the outer layer in both cross section and plan-view indicates a spatially nonuniform film density, consistent with nanoscale porosity in the hydrolyzed Zn−hybrid layer. The white arrow indicates one of several points in the plan-view image corresponding to a hollow hole through the film. These results suggest that the MLD hybrid organic/inorganic films may be useful as a precursor material to form well-defined conformal porous inorganic films and membranes.

4. Discussion

The results presented above show that while steady state self-limiting deposition is achieved during cyclic exposures of diethyl zinc and ethylene glycol, the DEZ mass uptake (∼20.4 ng/cm^2) is significantly less than the 125 ng/cm^2 obtained during DEZ exposure for ZnO ALD at 120 °C. This suggests that the density of reactive surface sites produced during the EG step in the steady-state MLD process is considerably less than that produced during H_2O exposure during steady-state ZnO ALD. In addition, the estimated saturated growth rate of the Zn−hybrid material (<2 Å/cycle) is considerably less than the length of ethylene glycol (5.3 Å), further confirming that the Zn−hybrid film does not grow as a series of fully extended organic monolayers. It is important to note, however, that the ratio of the mass uptake measured during DEZ and EG exposure throughout steady state Zn−hybrid film growth (20.4/4.8, in ng/(cm^2·cycle)) was close to the ratio expected from Scheme 2 (93/31, in g/(mol cycle)), taking into consideration the relatively large uncertainty in the QCM measurements for small mass changes. This self-consistent mass uptake ratio indicates that film growth is steady with time, and there is no net buildup of one reactant, or evolution of the film composition over time. Film growth has been extended to more than 800 cycles, showing long-term steady-state film deposition.

Table 1. Summary of Mass Uptake Results Obtained from QCM Analysis during Various ALD and MLD Half-Cycles on Starting Surfaces of Interest

conditions	exposure	mass uptake at 120 °C (ng/cm^2)	data
ZnO ALD steady state	H_2O	approx. −3	Figure 4
	DEZ	∼125 ± 3	Figures 2−4
ZnO ALD surface −OZn−OH saturated	H_2O	∼0	Figure 4
	EG	33	Figure 4
ZnO ALD surface −OZn−C_2H_5saturated	DEZ	∼0	Figure 2b
	EG	∼33	Figure 3a,b
ZnO ALD surface −OZnO−C_2H_4OH saturated	EG	∼0	Figure 3a,b
	DEZ	∼16	Figure 3a,b
MLD (−OZnO−C_2H_4−)$_n$ steady state	DEZ	∼20.4 ± 1.3	Figures 5−7
	EG	∼4.8 ± 1.4	Figures 5−7

Scheme 4

$$-\mathrm{Zn(OC_2H_4OH)(s)} + \mathrm{Zn(C_2H_5)_2} \rightarrow -\mathrm{OC_2H_4OZn(C_2H_5)(s)} + \mathrm{C_2H_6} \quad (6)$$

$$2[-\mathrm{Zn(C_2H_5)(s)}] + \mathrm{OHC_2H_4OH} \rightarrow -\mathrm{Zn-OC_2H_4O-Zn-(s)} + 2\mathrm{C_2H_6} \quad (7)$$

A summary of the mass uptake results is presented in Table 1, including values obtained during steady-state ZnO and Zn−hybrid deposition, and for the initial dose of EG on ZnO (after DEZ exposure) and for the initial dose of DEZ on ZnO (after exposure to one EG cycle). The mass uptake of DEZ in the Zn−hybrid film deposition is approximately the same during steady state and initial steps, but the EG shows a distinctly larger mass uptake in the early growth cycle as compared to steady state growth. When there is a significant density of reactive surface sites, for example after DEZ exposure during ZnO ALD, it is likely that a significant fraction of the glycol molecules undergo a "double reaction", where both hydroxyl moieties react with adjacent −OZn(C_2H_5)(s) surface sites to produce nonreactive Zn−ethylene oxide "bridging" groups, as shown in eq 7 in Scheme 4. This double reaction follows the same scheme proposed by Dameron et al. to account for mass uptake in aluminum/organic hybrid film deposition.[19]

The double reaction allows some EG molecules to passivate more than one active surface site. For a flat and dense ZnO ALD surface with material bulk density of ∼5.6 g/cm^3, the reactive site density is expected to be $\sim 1.2 \times 10^{15}$ cm^{-2} or approximately 3.2 Å between sites. Considering that the length of an EG molecule is ∼5.3 Å, a molecule that has reacted at only one end can access other available −Zn(C_2H_5)$_{(s)}$ surface sites within ∼5 Å to complete the double reaction, leaving isolate EG molecules separated by more than 5.3 Å. This corresponds to a surface site density of less than $\sim 3 \times 10^{14}$ cm^{-2} for the subsequent EG/DEZ surface reaction. Any dehydration reactions between single-reacted glycols, bound close enough to react with each other, will tend to further increase this mean separation distance and decrease the surface site density. This reduction in surface site density for the DEZ/EG reaction compared to the DEZ/H_2O process is evident in the QCM results. If the DEZ/EG reaction following Scheme 2 could achieve vertical self-assembly without significant double reaction, a mass gain of 124 g per mole of surface sites would be expected for each cycle, which is larger than the 79 g per mol from the DEZ/H_2O reaction in Scheme 1. Therefore, under fully dense vertically aligned film formation, the mass gain ratio would be approximated as (DEZ/EG)/(DEZ/H_2O) = 124/79 (in g/(mol cycle)) ≈ 1.6. However, the actual mass gain ratio is measured to be (DEZ/EG)/(DEZ/H_2O) = 24/125 (in ng/(cm^2·cycle)) ≈ 0.2 during the steady-state DEZ/EG deposition reaction, consistent with the double reaction in the DEZ/EG process (eq 7 in Scheme 4) acting to decrease the number of available reactive surface sites.

It is important to note that other mechanisms beyond the double reaction could be important in affecting the mass uptake rates. For example, the ethylene ligands can contribute steric effects, to effectively block available reactive sites.[16] It is also instructive to compare mass uptake values reported during alucone MLD[19] to those observed here. Because of the higher coordination of Al versus Zn and higher atomic density of Al_2O_3 versus ZnO, the TMA adsorption could be expected to produce a higher density of surface sites for EG adsorption as compared to DEZ. The mass uptake reported for EG adsorption during steady-state alucone MLD is between 8 and 17 ng/(cm^2·cycle) at 135 and 105 °C, which is larger than the value of ∼4.8 ng/(cm^2·cycle) reported here during MLD of zincone at 120 °C, consistent with a higher density of reactive surface sites for EG adsorption in the alucone MLD process.

5. Conclusions

Infrared transmission and quartz crystal microbalance analysis confirms that thin films of ZnO-organic hybrid polymer (−O−Zn−O−C_2H_4−)$_n$ material can be deposited from DEZ and ethylene glycol using an atomic/molecular layer deposition process over a range of substrate temperatures. In situ QCM analysis indicated that the sequential surface reactions of EG and DEZ are self-limiting and saturating, the Zn hybrid material deposition proceeds linearly, and film thickness increases with the number of deposition cycles. The mass uptake rate during Zn−hybrid film deposition decreased with increasing reaction temperature. The QCM results also indicate that the reaction mechanism of Zn hybrid films involves a significant amount of "double reaction" where the OH groups on both ends of the diol react with available −Zn(−C_2H_5)(s) surface sites to produce a relatively inert bridging alkane. The quantified mass uptake is consistent with a factor of ∼10 reduction in active surface site density during Zn−organic hybrid film

deposition compared to ZnO ALD at the same deposition temperature.

Infrared transmission demonstrates that Zn−organic hybrid films are stable in dry air. IR, XPS and ellipsometry results indicate that the materials react when exposed to humid laboratory air, releasing volatile organics resulting in ZnO films that are physically thinner, and contain C and OH reaction remnants. AFM and TEM analysis of the hydrolyzed Zn hybrid films show the material to be uniform and conformal, even in high-aspect-ratio structures, and the morphology of the TEM images indicate that the hydrolyzed Zn hybrid films contain uniform nanoscale porosity.

This work describes fundamental surface processes during atomic/molecular layer deposition of an example hybrid metal oxide−organic thin film. This method can be readily extended to other material systems including other diols, triols, or dicarboxylic acids reacting with a range of metal alkyls and other metal organics. These results suggest new pathways to fabricate organic−inorganic hybrid materials, including metal-organic framework structures, with well-defined conformality and film thickness, to enable many novel thin film materials with significant new applications.

Acknowledgment. This work was supported by the National Science Foundation under Grant CTS-0626256, and by the STC Program of the National Science Foundation under Agreement CHE-9876674. We are grateful to Ali Evren Ozcam, Shafi Mahmud Arifuzzaman, and Prof. Jan Genzer for spectroscopic ellipsometry measurements, Jeong-Seok Na for AFM measurements, Seymen Aygun, Michelle D. Casper, and Prof. J. P. Maria for XRD measurement, and Prof.'s Jan Genzer and Christopher Gorman for helpful discussions.

CM8020403